ELSEVIER

Journal of Alloys and Compounds 330–332 (2002) 718–722

Journal of ALLOYS AND COMPOUNDS

www.elsevier.com/locate/jallcom

Hydrogen absorption of nanocrystalline palladium

Toshiro Kuji[a,*], Yoshihito Matsumura[b], Hirohisa Uchida[b], Tatsuhiko Aizawa[c]

[a]*Corporate R&D Center, Mitsui Mining and Smelting Co. Ltd, 1333-2 Haraichi, Ageo, Saitama 362-0021, Japan*
[b]*Department of Applied Physics, Tokai University, 1117 Kitakaname, Hiratsuka, Kanagawa 259-1292, Japan*
[c]*Research Center for Advanced Science and Technology, University of Tokyo, 4-6-1 Komaba, Meguro-ku, Tokyo 153-8904, Japan*

Abstract

Thermodynamic properties of hydrogen in nanocrystalline Pd (Pd-n) were determined by pressure–composition (P–C) isotherms. Pd-n was prepared by repeated compression–extrusion cycles in the die cavity of a high speed forging apparatus. It was found that Pd obtained was composed of nano-sized Pd grains, i.e. ~10 nm, which were strained in ⟨111⟩ and ⟨100⟩ by 1.3 and 2.4%, respectively. From P–C isotherm measurements over the temperatures from 298 to 373 K, it was found that the hydrogen solubility in the α phase region for Pd-n was significantly larger than that for coarser grained Pd. On the other hand, Pd-n showed lower plateau pressures than coarser grained Pd. In addition to the above, the maximum hydrogen solubility of Pd-n was almost 50% lower than that for coarser grained Pd. The differences in the hydrogen solubility and plateau pressure between Pd-n and coarser grained Pd will be discussed under the consideration of the structure of nano-sized Pd grains. The drastic reduction in the maximum hydrogen solubility for Pd-n could be related to the viewpoint of strain of the octahedron in f.c.c. Pd.

Keywords: Nanocrystalline Pd; Hydrogen solubility; Thermodynamic properties; Strain

1. Introduction

Recently, great interest has focused on nanophase materials with ultrafine microstructures resulting in significantly different properties compared to conventional materials with coarser grains, implying the importance of not only the intrinsic properties but also of the extrinsic properties of materials. In this research field, a large number of studies concerned with the mechanical and magnetic properties of nanophase metals has been reported, demonstrating a remarkable improvement due to both grain-size and grain-boundary effects [1–4].

For hydrogen–metal systems, the effect of nano-scaled grains on the hydrogen absorbing behavior is also a very interesting research topic from both industrial and fundamental points of view. Nanostructural control could lead to a drastic improvement of the hydrogen absorption properties. For example, many previous works on $Mg_{2-x}Ni_x$ ($x=0-1$)–H systems have pointed out the importance of nano-sized structure control to improve the hydriding and dehydriding properties [5–8]. From the academic point of view, most research has focused interest on Pd–H system in ultrafine structured Pd [9–13] because Pd is a typical f.c.c. metal which can absorb a large amount of hydrogen. For this system, thermodynamic properties, i.e. plateau pressures and phase boundary envelopes, are substantially affected by the reduction in grain size. Even micro-scaled grains show quite different thermodynamic behavior compared to coarser grained Pd [14]. In the nano-scaled region, Mutschele and Kirchheim [9,10] have suggested that the hydrogen absorption and diffusion behavior in Pd-n can be understood by the existence of highly disordered grain boundary with large volume fraction in Pd-n. According to their model, a significant amount of hydrogen segregates in the grain boundaries and the segregated hydrogen could not be transformed into the β phase. However, recent investigations on Pd-n by Thomas et al. [15,16] using high-resolution electron microscopy concluded that the Pd-n grain boundary is not highly disordered, contrary to the results of earlier X-ray studies [17].

More recently Eastman and co-workers have reported narrowing of the Pd–H phase envelope in Pd-n and anticipated that strain in ultrafine grains could be responsible for the change in the thermodynamic quantities [13]. However, clear interpretation of the thermodynamic properties of hydrogen in Pd-n has not been available yet. In this study, the thermodynamic properties obtained from P–C isotherms for Pd-n will be discussed from the

*Corresponding author.
E-mail address: t_kuji@mitsui-kinzoku.co.jp (T. Kuji).

0925-8388/02/$ – see front matter
PII: S0925-8388(01)01597-3

viewpoint of strain of the interstitial octahedron in f.c.c. Pd.

2. Experimental

Nanocrystalline Pd (Pd-n) investigated in the present study was prepared by repeatedly extruding and compressing Pd in a die cavity of high speed forging apparatus. This apparatus was originally designed for bulk mechanical alloying (BMA) as a new conceptual mechanical alloying instead of the conventional MA based on ball milling or attrition. Pd fragments by cutting Pd sheets with 99.99% purity were poured into a die cavity of 25-mm diameter. The amount of Pd to be processed was ~25 g. The Pd fragments were repeatedly extruded and compressed by maximum applied load of 500 kN in the die cavity. One extrusion–compression cycle took ~8 s. In this study, the Pd fragments were processed for 1500 extrusion–compression cycles. The forging facilities and cyclic loading schedule have been described in detail elsewhere [8,18]. From the above process, the Pd sample with ultrafine Pd grains was prepared in bulk shape with ~80% of Pd ingot density.

The compacted materials were characterized by X-ray diffraction using Cu radiation at room temperature. The microstructures were investigated using transmission electron microscopy (TEM). The *P–C* isotherms were determined using a Sievert's apparatus at 298–373 K.

3. Results and discussion

Fig. 1 shows X-ray diffraction patterns of ultrafine grained Pd used in this study. Each diffraction peak from Pd with ultrafine grains was located at slightly lower diffraction angles than that for Pd with coarser grains. In fact, calculated lattice parameter of nano-grained Pd, $a=3.927$ Å is slightly larger than the value for coarser grained Pd, $a=3.891$ Å. Fig. 2 shows the high-resolution transmission electron micrograph (TEM) of Pd with ultrafine grains. From the lattice image it can be said that the highly disordered grain boundary phase, as suggested by Mutschele and Kirchheim [9,10], could not be observed in TEM micrograph. It was difficult to confirm the existence of the highly disordered grain boundary phase but if the fraction of highly disordered phase is significant in the total volume of Pd-n, it could be said that the background intensity in X-ray diffraction should be more diffuse.

In this study, the grain size for Pd with ultrafine grains was determined by X-ray diffraction analysis of line broadening. Calculated grain size was 8 nm, in good agreement with value from TEM observations, which was estimated to be more or less 10 nm. The internal strain in ultrafine grain was also calculated from the X-ray diffraction peak broadening. It was found that lattice strains in ⟨111⟩ and ⟨100⟩ directions are 1.3 and 2.4%, respectively. It is believed that these anisotropic strain values are not affected by the presence of the highly disordered grain boundary.

Fig. 3(a,b) shows *P–C* isotherms for Pd-n and conventional coarser grained Pd at 298–373 K. The phase boundary of the Pd–H miscibility gap is significantly narrower for Pd-n than for coarser grained Pd. The hydrogen solubility at $\alpha/(\alpha+\beta)$ phase boundary is significantly increased and the hydrogen solubility at $(\alpha+\beta)/\beta$ phase boundary is drastically reduced in Pd-n. Moreover, the maximum hydrogen concentration in β phase for Pd-n is reduced by almost 50%. This means that 50% of available interstitial sites disappeared in Pd-n or the

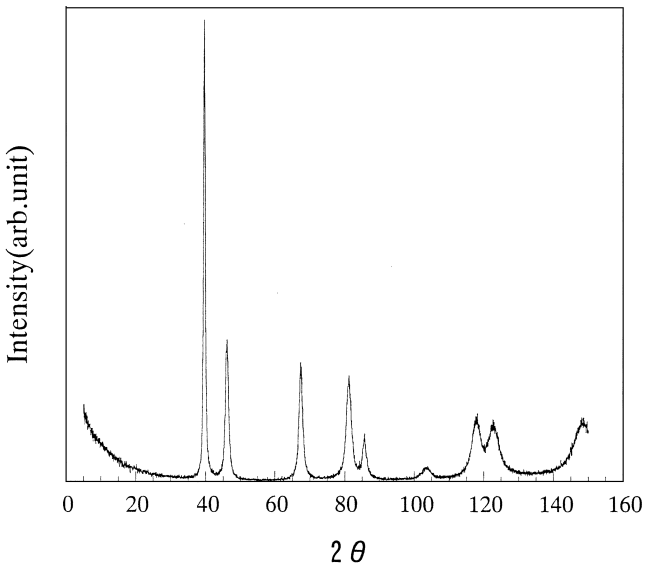

Fig. 1. X-ray diffraction pattern for the nanocrystalline Pd.

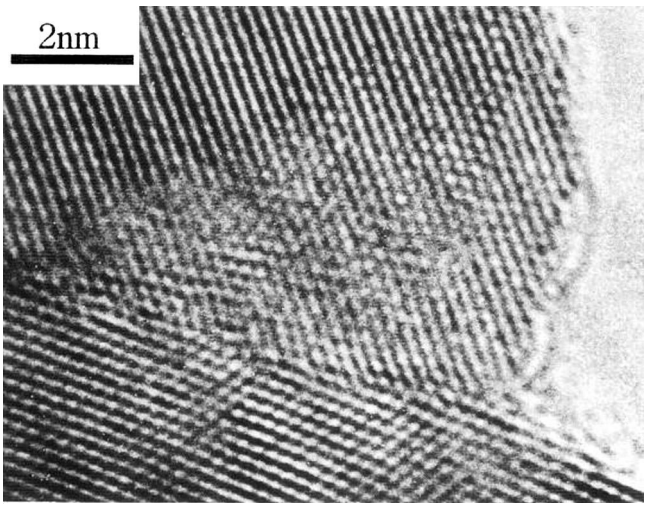

Fig. 2. High resolution transmission electron micrograph of nanocrystalline Pd.

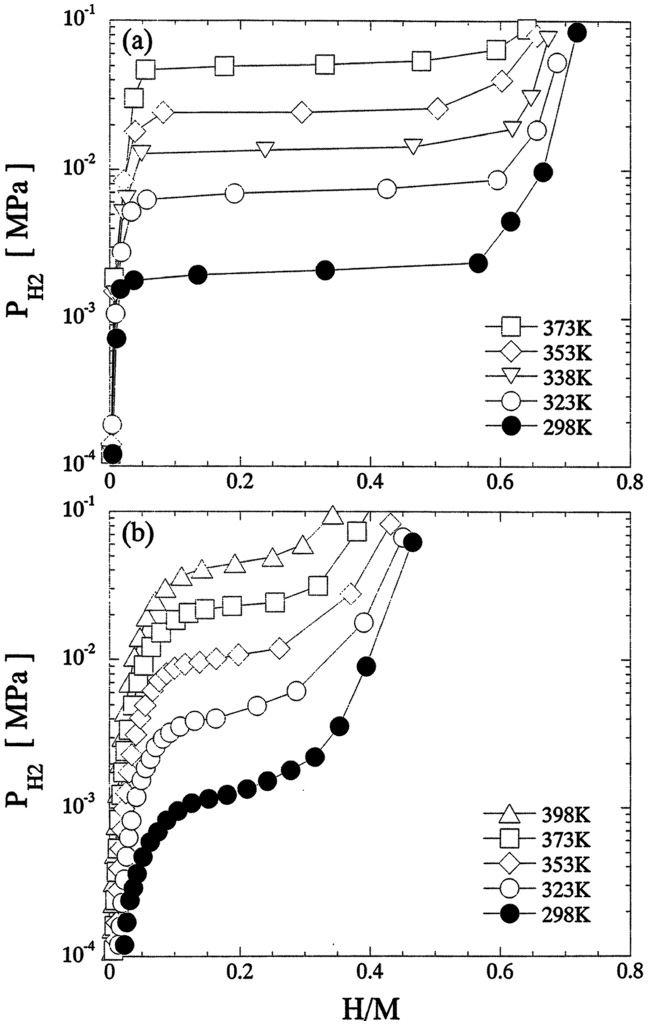

Fig. 3. Pressure–composition isotherms for coarser grained Pd (a) and nanocrystalline Pd (b).

distribution of interstitial site energy was broadened to higher energy region.

The chemical potentials of hydrogen in gas and Pd, μ_{H_2} and μ_H, are given by

$$1/2\mu_{H_2} = 1/2\mu^0_{H_2} + RT \ln P^{1/2}_{H_2} \quad (1)$$

$$\mu_H = \mu^0_H + RT \ln(r/(\beta - r)) + \mu^E_H \quad (2)$$

where r=(mol H/mol Pd), μ^0_H is the chemical potential of hydrogen in the hypothetical infinitely dilute solution and μ^E_H is the excess chemical potential of hydrogen. From Eqs. (1) and (2) at equilibrium between metal and hydrogen gas, we obtain

$$RT\ln\{P^{1/2}_{H_2}((\beta - r)/r)\} = \Delta\mu^0_H + \mu^E_H \quad (3)$$

where $\Delta\mu^0_H = \mu^0_H + 1/2\mu^0_{H_2}$, which is the chemical potential of hydrogen at $r \to 0$. The hydride formation for the Pd–H system takes place in the miscibility gap type of transformation so that each thermodynamic parameter in Eqs. (1)–(3) varies continuously with temperature and/or hydrogen concentration. The values of $\Delta\mu^0_H$ and μ^E_H can be separately obtained by plotting the left hand side of Eq. (3) against r [14,19]. In the present work, in order to simplify the above thermodynamics without losing the generality, the regular solution approximation was applied for the α solid solution region so that Eq. (2) can be rewritten as

$$RT \ln\{P^{1/2}_{H_2}((\beta - r)/r)\} = \Delta\mu^0_H + W_{HH}r \quad (4)$$

where W_{HH} is coefficient determined from the zeroth approximation of the excess chemical potential of hydrogen. The Curie temperature, Tc of miscibility gap can be obtained from the condition $\partial\mu H/\partial r = 0$ and $\partial^2\mu H/\partial r^2 = 0$, as

$$T_c = -\beta W_{HH}/4R \quad (5)$$

where β is the maximum hydrogen solubility in Pd. In the case of Pd–H system, hydrogen atoms occupy the octahedral sites of f.c.c. Pd so that $\beta = 1.0$. The ratio of T_c(nano) to T_c(coarse) can be written as

$$T_c(\text{nano})/T_c(coarse) = \beta_n W_{HH}(\text{nano})/\beta_c W_{HH}(\text{coarse}) \quad (6)$$

where β_n and β_c are values of β for Pd-n and coarser grained Pd, respectively. T_c(coarse) is well known as $T_c = 570$ K [20–22]. At temperatures below T_c, the hysteresis appears in plateau region on isotherms because of the existence of the difference phase boundary during the hydride formation and decomposition processes, but it should disappear at temperatures above T_c. In this study, T_c(nano) was, therefore, determined from the logarithmic plots of absorption and desorption plateaus against reciprocal temperature. Two straight lines were obtained as shown in Fig. 4. The intersection of the two straight lines should correspond to T_c. In the present work, T_c(nano) was estimated to be ~435 K, which is far below T_c(coarse), so that Eq. (6) can be rewritten as

$$\beta_n W_{HH}(\text{nano}) = 0.76\beta_c W_{HH}(\text{coarse}) \quad (7)$$

where $0.75 = T_c(\text{nano})/T_c(\text{coarse}) = 435$ K/570 K. If Eq. (6) is valid with $\beta_n < 1$ for Pd-n, $(1-\beta_n)$ interstitial sites per Pd-n would be no longer available for hydrogen occupation in Pd-n. In the present work, when $\beta_n > 0.9$ for Pd-n, both sides of Eq. (7) gave almost same value, although accuracy of hydrogen solubility at low hydrogen concentration region is relatively low. Fig. 5 shows the plot of $\chi\beta RT \ln\{P^{1/2}_{H_2}((\beta - 1)/r)\}$ against r at 373 K, where $\chi = 1.0$, $\beta_n = 0.9$ for Pd-n and $\chi = 0.76$, $\beta_c = 1.0$ for coarser grained Pd. The slope of each line corresponds to the value of either left- or right-hand side of Eq. (7). It can be seen that slopes of both lines are almost identical, indicating $0.9W_{HH}(\text{nano}) = 0.76W_{HH}(\text{coarse})$. This means that T_c for the Pd-n is lower by 135 K than T_c for the coarser grained Pd and almost all interstitial sites in Pd-n are still available for hydrogen occupation because the value of β_n for Pd-n is close to 1.0. This suggests that

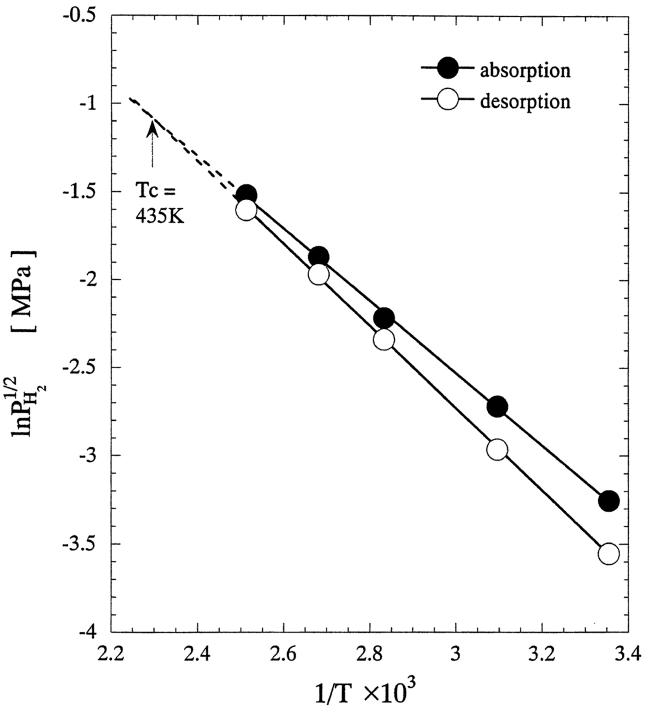

Fig. 4. Van't Hoff plot of absorption and desorption plateaus for nanocrystalline Pd.

$r = 1.0$ of the maximum hydrogen solubility in Pd-n should be obtained at higher equilibrium hydrogen pressure.

In this study, the strain of the octahedron in f.c.c. Pd was considered to interpret the difference in the thermodynamic properties between nanocrystalline and coarse grained Pd as discussed above. Fig. 6 shows a schematic illustration of the octahedron for hydrogen occupation in f.c.c. Pd. As mentioned previously, Pd nanograins are strained by 1.3 and 2.4% along ⟨111⟩ and ⟨100⟩ directions, respectively. In the present study, the interstitial volume was defined as the diameter of largest sphere inscribed in the octahedron which is $0.828 r_{Pd}$ where r_{Pd} is the atomic radius (CN12) of Pd. The value of $0.828 r_{Pd}$ can be calculated from the inter-atomic distance between Pd atoms under the consideration of the Pd atomic radius. If the octahedron is elongated along ⟨100⟩ direction, Pd atoms on (0,0,2) plane, perpendicular to ⟨100⟩ direction, move towards the center of the octahedron due to the existence of Poisson's ratio. Consequently, the b–d and a–f distances become shorter, with the result that effective volume of octahedron becomes smaller. Therefore, it can be concluded that the ⟨100⟩ elongation yields reduction in the effective octahedron volume, which means that the site energy for hydrogen occupation is higher, so that hydrogen occupation is expected to become more difficult. In the case of shrinkage along ⟨100⟩ direction, the effective volume again becomes smaller even though the b–d and a–f distances are longer, which is the reverse of the case for the ⟨100⟩ elongation, so that hydrogen occupation becomes more difficult (higher site energy) after the shrinkage. On the other hand, ⟨111⟩ elongation yields the increase in the distance between planes 'cdf' and 'abe', resulting in the increase in the b–d distance. Therefore, the octahedron volume increases so that the site energy

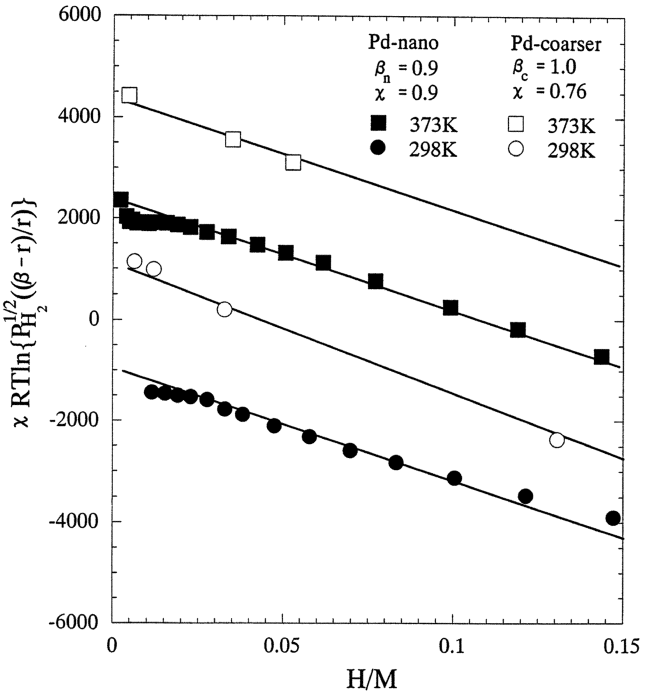

Fig. 5. Plot of $RT\ln\{P_{H_2}^{1/2}((\beta - r)/r)\}$ against $r = H/Pd$.

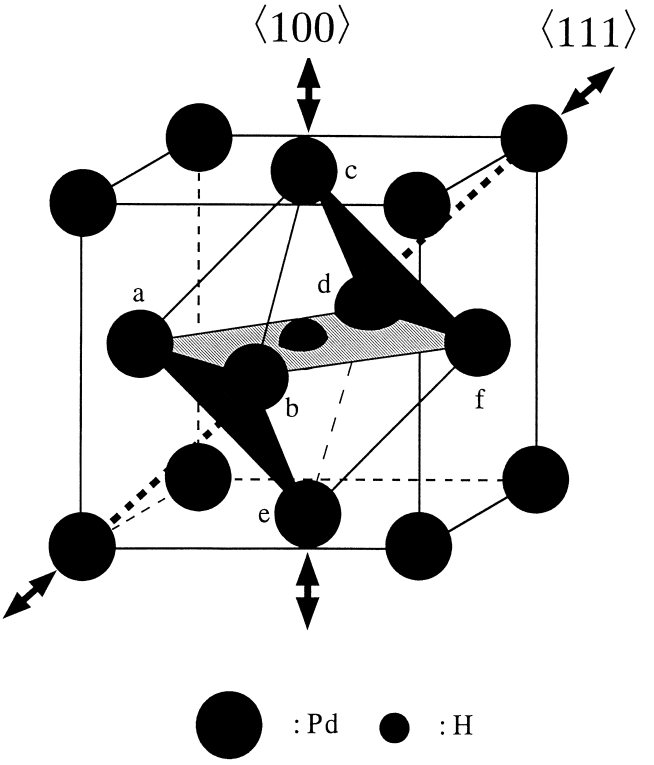

Fig. 6. Schematic illustration of octahedron in f.c.c. Pd.

becomes lower. In the case of the ⟨111⟩ shrinkage, higher site energy (more difficult to be occupied) can be expected.

As discussed above, the strain in grain interior causes the broadening of the site energy distribution. The hydrogen atoms are distributed over interstitial sites with different site energy. The difference in site energy is created from the change in local environments around position to be occupied by hydrogen atom. In amorphous alloys, the site energy distribution is typically continuous due to the continuous variation in the configuration of atoms [23,24]. In the case of the f.c.c. Pd, there are three and four equivalent directions to ⟨100⟩ and ⟨111⟩, respectively. Moreover, the magnitude of strain is distributed, for example, from −2.4% (shrinkage) to +2.4% (elongation) in ⟨100⟩, corresponding to the strain calculated from X-ray diffraction peak width. The statistics on the strain distribution over a large number of grains may suggest that the site energy could be also continuously distributed.

The broadening of the site energy distribution is directly reflected on T_c [25,26]. Reduction in T_c for Pd-n by 135 K, shown in Fig. 4, could be the evidence that the site energy distribution is significantly broadened in Pd-n. The broadening of the site energy to lower energy region directly yields the increase in hydrogen concentration in α phase, i.e. case of ⟨111⟩ elongation. On the other hand, the decrease in hydrogen concentration in β phase is caused by the broadening to higher energy region, i.e. cases of ⟨111⟩ shrinkage and both ⟨100⟩ elongation and shrinkage. In conclusion, The difference in the thermodynamic properties between Pd-n and coarser grained Pd could be, therefore, interpreted by the broadening of the site energy distribution caused by strain of grain interior.

4. Conclusions

In the present study, the thermodynamic properties of hydrogen in nanostructured Pd (Pd-n) were determined from pressure–composition isotherms. Nanostructured Pd (Pd-n) was prepared by repeated extrusion–compression cycles. It was found that nano-sized Pd grains were strained in ⟨111⟩ and ⟨100⟩ directions by 1.3 and 2.4%, respectively. Because the atomic local environment around the interstitial site changes by the anisotropic strain of nano-sized grain, it could be expected that the site energy distribution is broadened. In this study, it was shown that the difference in thermodynamic properties, Curie temperature, hydrogen solubilities in α phase and β phase between Pd-n and coarser grained Pd could be interpreted by the site energy broadening.

Acknowledgements

This study was supported by a Grant-in-Aid for Scientific Research on Priority Area A of 'New Protium Function' of the Ministry of Education, Science, Sports and Culture, Japan. The authors acknowledge valuable discussions with Dr Y. Aoki, Corporate R&D Center, Mitsui Mining and Smelting Co. Ltd. Furthermore, we are indebted to Ms. Yamamuro, student of Tokai University for her careful measurements of *P–C* isotherms and Ms. Hanzawa, Corporate R&D Center, Mitsui Mining and Smelting Co. Ltd for HRTEM observations.

References

[1] E.F. Kneller, F.E. Luborsky, J. Appl. Phys. 34 (1963) 656.
[2] S. Gangopadhyay, G.C. Hajdjipanayis, S.I. Shah, C.M. Sorensen, K.J. Klabunde, V. Papaefthymiou, A. Kostikas, J. Appl. Phys. 70 (1991) 5888.
[3] A.H. Chokshi, A. Rosen, J. Karch, H. Gleiter, Scripta Metall. 23 (1989) 1689.
[4] G.W. Nieman, J.R. Weertman, R.W. Siegel, J. Mater. Res. 6 (1991) 1012.
[5] S. Orimo, H. Fujii, J. Alloys Comp. 232 (1996) L16.
[6] Z. Dehouche, R. Djaozandry, J. Goyette, T.K. Bose, J. Alloys Comp. 288 (1999) 312.
[7] T. Spassov, U. Koster, J. Alloys Comp. 287 (1999) 243.
[8] T. Aizawa, T. Kuji, H. Nakano, J. Alloys Comp. 291 (1999) 248.
[9] T. Mutschele, R. Kirchheim, Scripta Metall. 21 (1987) 135.
[10] T. Mutschele, R. Kirchheim, Scripta Metall. 21 (1987) 1101.
[11] A. Pundt, C. Sachs, M. Winter, M.T. Reetz, D. Fritsch, R. Kirchheim, J. Alloys Comp. 293–295 (1999) 480.
[12] A.L. Bonivardi, M.A. Baltanas, J. Catal. 138 (1992) 500.
[13] J.A. Eastman, L.J. Thompson, B.J. Kestel, Phys. Rev. 48 (1993) 84.
[14] T. Kuji, H. Uchida, M. Sato, W. Cui, J. Alloys Comp. 293–295 (1999) 19.
[15] G.J. Thomas, R.W. Siegel, J.A. Eastman, Mater. Res. Soc. Symp. Proc. 153 (1989) 13.
[16] G.J. Thomas, R.W. Siegel, J.A. Eastman, Scripta Metall. 24 (1990) 201.
[17] T. Houbold, R. Birringer, B. Lengeler, H. Gleiter, Phys. Lett. A 135 (1989) 461.
[18] T. Aizawa, C. Zhou, Adv. Eng. Mat. 2 (2000) 29.
[19] T. Kuji, W.A. Oates, J. Phys. F: Met. Phys. 13 (1983) 1785.
[20] H. Frieske, E. Wicke, Ber. Bunsenges. Phys. Chem. 77 (1973) 50.
[21] Y. de Ribaupierre, F.D. Manchester, J. Phys. C: Sold State Phys. 7 (1974) 2126.
[22] T.B. Flanagan, T. Kuji, W.A. Oates, J. Phys F: Met. Phys. 15 (1985) 2273.
[23] R. Kirchheim, Acta Metall. 21 (1973) 1233.
[24] R. Kirchheim, Acta Metall. 30 (1982) 1069.
[25] R. Griessen, Phys. Rev. B 27 (1983) 7575.
[26] Y. Fukai, The Metal-hydrogen System, Basic Bulk Properties, Springer-Verlag, Berlin, Heidelberg, 1992.